

## **TRAVELLING-WAVE MODELLING OF UNIFORM MULTI-CONDUCTOR TRANSMISSION LINE NETWORKS — PART II: EXPERIMENTAL VALIDATION — APPLICABILITY**

**Ioannis C. Papaleonidopoulos<sup>\*</sup>, Nickolas J. Theodorou, and Christos N. Capsalis**

School of Electrical and Computer Engineering, National Technical University of Athens, 9 Heroon Polytechniou str., Zografou, Athens 15780, Greece

**Abstract**—In Part I of this work, travelling-wave modelling of uniform multi-conductor transmission line networks was analytically established with direct applicability to narrowband transmission, covering any network formed of lossy (in the general case), diagonalisable uniform multi-conductor transmission lines of either distinct or degenerate eigenvalues. As the whole work applies especially in the field of Power-Line Communications, in Part II, a validating experimental paradigm is first provided using a common cable type for indoor power electric networks. Then, direct applicability to narrowband transmission is addressed, along with potential expandability towards wideband signalling. A comparative evaluation with other existing methods of time-domain modelling is also included and relevant directions for future research are suggested.

### **1. INTRODUCTION**

The travelling-wave modelling of uniform multi-conductor transmission line (MTL) networks, which was analytically established in Part I of this work, has already been verified for the two-conductor transmission-line (TL) sub-case — as defined under Subsection 6.2.2 therein — in [1] and [2], via computational simulation and experimental validation of the output results on amplitude-response basis. In both aforesaid works, the approach was to evaluate and confirm the

---

*Received 20 January 2013, Accepted 10 May 2013, Scheduled 10 June 2013*

<sup>\*</sup> Corresponding author: Ioannis C. Papaleonidopoulos (jppap@central.ntua.gr).

extent to which the set of all *paths* (considered in [1] and [2] to be the several travelling-wave components, same as defined in Part I of this work, Subsections 4.1.2.3 and 4.1.3.2 therein) lying within two (2) orders of magnitude below the direct one, of which the propagation route comprises no reflections, is sufficient to accurately calculate the transfer properties of the examined channels. In [1], the above path-inclusion criterion was approximately approached and provided minimum amplitude-response accuracy of 10 dB, whereas exact application of the same criterion ensured in [2] a minimum amplitude-response accuracy of 5 dB.

In this paper (Part II), the travelling-wave modelling established in Part I is experimentally verified for the general MTL case, and in particular over a 5-conductor TL network. The notation introduced in Part I is also followed throughout this paper. The validating paradigm is provided in Section 2. An explanatory discussion on applicability follows in Section 3 in terms of the type of transmission (narrowband or wideband) and frequency variation of the medium, along with an evaluative outline of the comparative novel assets of this travelling-wave approach and the resulting exploitation prospects. A concluding summation closes the paper in Section 4.

## 2. EXPERIMENTAL VALIDATION

### 2.1. Measuring Methodology

The validation has been conducted via amplitude-response measurements over a bus (i.e., a MTL cable) with transverse open-circuited branches coupled in parallel, as in Figure 1. The branches are num-

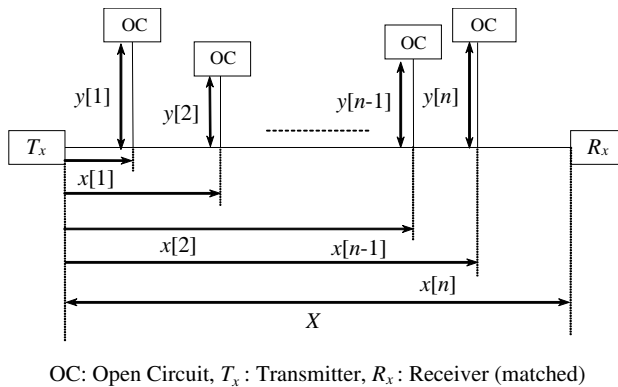


**Figure 1.** Test channel configuration.

bered consecutively from transmitter to receiver. Denoting by  $x[i_b]$  the distance of the  $i_b$ -branch intersection from the bus origin,  $y[i_b]$  the length of the  $i_b$ -th branch and  $X$  the bus length, the test channel topology is described as:  $n = 2$ ,  $X = 18$  m,  $\mathbf{x} = [5.0$  m  $13.0$  m] $^T$ , and  $\mathbf{y} = [3.0$  m  $2.0$  m] $^T$ , which means that two (2) branches of lengths 3.0 m and 2.0 m have been coupled at 5.0 m and 13.0 m respectively from the transmission end (i.e., the origin  $T_x$ ), whereas the overall bus length from transmission end to reception end (i.e., the end  $R_x$ ) is 18 m. The experimental power-line circuitry was assembled of the common  $5 \times 1.5$  mm $^2$  NYM per VDE 250 three-phase flexible power cable of five (5) identical insulated wires at symmetric cross-sectional arrangement inside an insulating sheath, as shown in Figure 2.

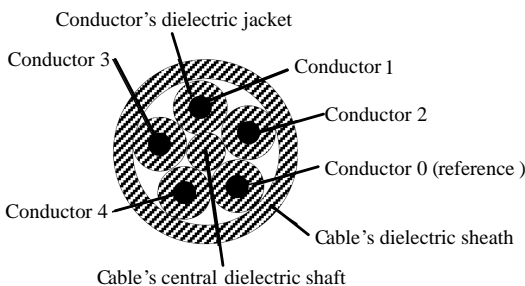


**Figure 2.** Cross section of the NYM  $3 \times 1.5$  mm $^2$  cable.

With reference to the cable structure of Figure 2, the transmission circuit between Conductor 1 (excitation conductor) and Conductor 0 (reference) was selected. An Agilent 33250A sweep/function generator configured at  $\hat{Z}_{G_{10}} = |\hat{Z}_{G_{10}}| = 50 \Omega$  output resistance was used to provide the sinusoidal excitation voltage, and was coupled at transmitter ( $T_x$ ,  $x = 0$ ) between the two aforesaid conductors. At the receiver ( $R_x$ ,  $x = X = 18$  m), a  $\hat{Z}_L = |\hat{Z}_L| = 68.6 \Omega$  metal film (M/F) resistive element was connected in parallel with a Tektronix TDS 210 digital double-channel oscilloscope, where input and output voltages (i.e., at the  $T_x$  and  $R_x$  positions respectively) were observed throughout 1.6–25 MHz at 100 kHz steps, of which the amplitude ratio was recorded as the *measured amplitude response* that corresponds to the resultant at  $T_x$  and  $R_x$  line voltage quantities represented in Equation (54a) of Part I.

The equipment was coupled at transmission ( $T_x$ ) and reception ( $R_x$ ) as depicted in Figure 3. Input impedance of the specific oscilloscope is for both channels equal to a  $1 \text{ M}\Omega \pm 2\%$  resistor in parallel with a  $(20 \pm 3)$  pF capacitor.

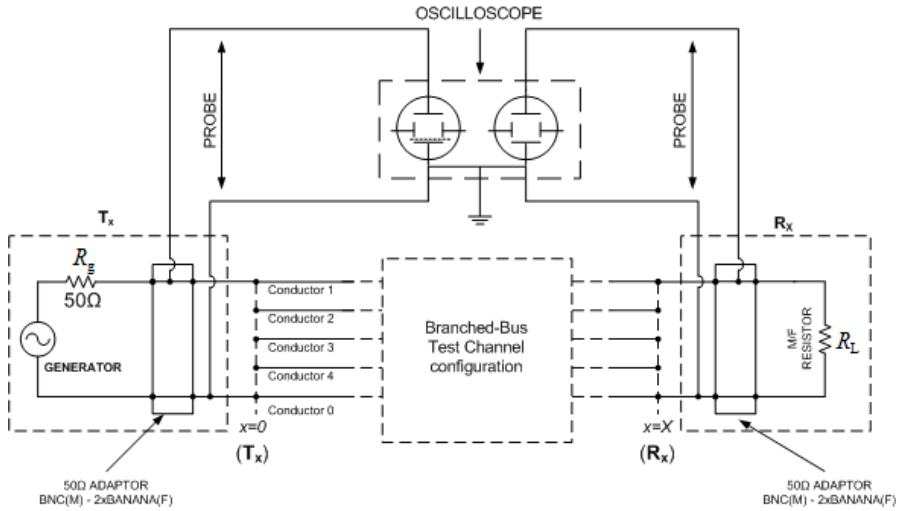


**Figure 3.** Equipment circuitry at transmission and reception.

To completely clarify the configuration of the experimental set-up, and with reference to Figures 1 to 3, it should additionally be noted that:

- 1) At the channel's origin ( $T_x$ ) and end ( $R_x$ ), only conductors 1 and 0 are coupled to the generator and the M/F resistive load respectively, whereas conductors 2, 3 and 4 remain open circuited, as shown in Figure 3.
- 2) At the end of the transverse branches, all five (5) conductors of the cable remain open circuited (OC), as indicated in Figure 1.
- 3) The two (2) transverse branches that were actually included in the measured channel between transmission ( $T_x$ ) and reception ( $R_x$ ) were coupled at the aforesaid positions  $\mathbf{x}[1] = 5\text{ m}$  and  $\mathbf{x}[2] = 13\text{ m}$  *in parallel*, i.e., Conductor 1 of the branch cable with Conductor 1 of the cable connecting  $T_x$  with  $R_x$  (the bus cable), Conductor 2 of the branch cable with Conductor 2 of the bus cable and so on.

## 2.2. Multiconductor Transmission Line Model

In terms of the MTL model defined in Part I, the experimental circuitry represents a 5-conductor TL network ( $\nu = 4$ ) arranged as in Figure 1, where the *termination admittance matrices* (TAMs) at channel's origin

$(T_x)$  and end  $(R_x)$  are respectively:

$$[\hat{\mathbf{Y}}_0]_{kk'} = \left\{ \begin{array}{l} |\hat{Z}_{G_{10}}|^{-1}, \quad (k, k') = (1, 0) \\ 0, \quad (k, k') \neq (1, 0) \end{array} \right\}, \quad k, k' = 1, \dots, 4 \quad (1a)$$

$$[\hat{\mathbf{Y}}_L]_{kk'} = \left\{ \begin{array}{l} |\hat{Z}_L|^{-1}, \quad (k, k') = (1, 0) \\ 0, \quad (k, k') \neq (1, 0) \end{array} \right\}, \quad k, k' = 1, \dots, 4 \quad (1b)$$

In order to extract a MTL model for the  $5 \times 1.5 \text{ mm}^2$  NYM cable, the wide-separation approximation suggested in [3] is assumed. Some additional inaccuracy is thus inserted, as (i) proximity effects are not taken into account, and (ii) supposing all five (5) conductors to lie in homogeneous dielectric, dielectric-constant transitions within the cable cross section are ignored. This latter approximation is well reasonable, since not only the air gaps in between the dielectric sections (jacket, shaft, and sheath) are indeed narrow, but it has as well been experimentally justified for the three-conductor NYM cable in [2] and [4]; the former one though (ignorance of proximity effects) is to be evaluated from the experimental-verification results presented here below. By virtue of the aforementioned assumptions, the distributed parameter matrices defined in Equation (1) of Part I, i.e., the per-unit-length resistance, inductance, capacitance, and conductance  $4 \times 4$  matrices become respectively from [3]:

$$\mathbf{R} = R \begin{bmatrix} 2 & 1 & 1 & 1 \\ 1 & 2 & 1 & 1 \\ 1 & 1 & 2 & 1 \\ 1 & 1 & 1 & 2 \end{bmatrix}, \quad R = \frac{1}{2r} \sqrt{\frac{\mu_r \mu_0 f}{\pi \sigma_w}} \quad (2a)$$

$$\mathbf{L} = \mathbf{L}_{in} + \mathbf{L}_{ex}, \quad \mathbf{L}_{in} = (2\pi f)^{-1} \mathbf{R}, \quad \mathbf{L}_{ex} = \mu_r \mu_0 \mathbf{F} \quad (2b)$$

$$\mathbf{C} = \varepsilon_r \varepsilon_0 \mathbf{F}^{-1} \quad (2c)$$

$$\mathbf{G} = 2\pi f \tan \delta \mathbf{C} \quad (2d)$$

$$[\mathbf{F}]_{kk'} = \left\{ \begin{array}{l} \frac{1}{2\pi} \ln \left( \frac{d_{k0}^2}{r^2} \right), \quad k = k' \\ \frac{1}{2\pi} \ln \left( \frac{d_{k0} d_{k'0}}{d_{kk'} r} \right), \quad k \neq k' \end{array} \right\}, \quad k, k' = 1, \dots, 4 \quad (2e)$$

where  $r$  is the conductors' radius,  $d_{kk'} \{k, k' = 0, \dots, 4\}$  the cross-sectional distance between the centres of conductors  $k$  and  $k'$ ,  $\sigma_w$  the conductivity of the conductors' material (Cu),  $\varepsilon_r$  and  $\mu_r \cong 1$  the relative dielectric permittivity and relative magnetic permeability respectively of cable's dielectric (PVC), and  $\tan \delta$  its dissipation factor (loss tangent).

From (2), the per-unit-length impedance and admittance matrices

defined in Equation (4a) of Part I become respectively:

$$\hat{\mathbf{Z}} = (1 + j)\mathbf{R} + j2\pi f\mu_0\mathbf{F} \quad (3a)$$

$$\hat{\mathbf{Y}} = 2\pi f\varepsilon_r\varepsilon_0(\tan\delta + j)\mathbf{F}^{-1} \quad (3b)$$

and provide:

$$\hat{\mathbf{Z}}\hat{\mathbf{Y}} = 2\pi f\varepsilon_0\varepsilon_r[(1 + j)(\tan\delta + j)\mathbf{R}\mathbf{F}^{-1} - 2\pi f\mu_0(1 - j\tan\delta)\mathbf{I}_4] \quad (4a)$$

$$\hat{\mathbf{Y}}\hat{\mathbf{Z}} = 2\pi f\varepsilon_0\varepsilon_r[(1 + j)(\tan\delta + j)\mathbf{F}^{-1}\mathbf{R} - 2\pi f\mu_0(1 - j\tan\delta)\mathbf{I}_4] \quad (4b)$$

where  $\mathbf{I}_4$  is the  $4 \times 4$  unit matrix. Both matrices (4a) and (4b) have the same, frequency-dependent couple of double-multiplicity degenerate eigenvalues, but due to the structure of matrices  $\mathbf{F}$  and  $\mathbf{R}$ , diagonalisation can indeed be achieved in a frequency-independent way. Substituting in (2) the actual conductor radius  $r = 0.691$  mm, and as thickness of the conductor jackets was measured at 0.8 mm, the voltage transformation matrix is reduced at three (3) significant digits as:

$$\hat{\mathbf{T}}_V = \mathbf{T}_V = \begin{bmatrix} 1 & 0.861 & 0.400 & 0.618 \\ 0.618 & 0.861 & -0.861 & 0.618 \\ 0.618 & 0 & -0.861 & 0 \\ 0 & -0.531 & 0 & 1 \end{bmatrix} \quad (5a)$$

and the corresponding current transformation matrix is calculated from Equation (6c) of Part I as:

$$\hat{\mathbf{T}}_I = \mathbf{T}_I = \begin{bmatrix} 0.777 & 0 & 0.558 & 0 \\ -0.777 & 0.841 & -0.558 & 0.447 \\ 1.138 & -0.841 & -0.345 & -0.447 \\ 0 & -0.520 & 0 & 0.724 \end{bmatrix} \quad (5b)$$

As far as material parameters are concerned, the values of Table 1 are considered, same as in [2] and [4].

**Table 1.** Material parameters.

Parameter	Value
$\varepsilon_r$	$-0.88 \log f + 9.50$ , $1$ , $6 \text{ MHz} \leq f < 5 \text{ MHz}$ $-3.3 \cdot 10^{-9} f + 3.61$ , $5 \text{ MHz} \leq f < 30 \text{ MHz}$
$\mu_r$	1.0
$\tan\delta$	$-5$ , $7 \cdot 10^{-10} f + 0.085$
$\sigma_w$	$5.80 \cdot 10^{-7} \text{ S/m}$

### 2.3. Simulation and Results

To obtain the results theoretically anticipated from the travelling-wave analysis, an algorithm that simulates the response estimation procedure suggested in Subsection 6.1 of Part I has been developed and computationally implemented for the branched-bus network topology of Figure 1, incorporating though the following additional approximations:

- 1) Only the real part of the initially excited modal quantities  $\tilde{V}_{m\xi 0}^+(t)$ ,  $\xi = 1, \dots, 4$ , as defined in Equation (37) of Part I, is considered, which is time-invariant due to the sinusoidal input.
- 2) Only the real part of the  $4 \times 4$  *modal travelling transmission coefficient matrix* (MTRCM) defined in Equation (47c) of Part I is considered.

Since respective imaginary parts result in both above cases no less than two (2) order of magnitudes below the homologous real ones, that couple of approximations seem rather reasonable.

The measured and simulated results are comparably illustrated in Figure 4, where the dashed line is obtained after aggregating all the several travelling components within two (2) orders of magnitude below the main (in magnitude terms) direct path, i.e., of which the propagation route from  $T_x$  to  $R_x$  involves no reflections, according to Equation (54a) of Part I.

No deviation above 7.5 dB is observed between theoretical and measured curves, whereas throughout most of the 1.6–25 MHz band examined, the observed deviation is much lower, around 2–3 dB or even less. Increase of deviation up to 4–7 dB that is spotted over certain narrow frequency areas should probably be attributed to the wide-separation assumption, as well as to excessive variation of the material parameters and the lumped termination resistor at  $R_x$  as frequency increases, as indicated by the fact that above 18 MHz, somewhat higher deviation seems to be established.

From a qualitative point of view, validity of the travelling-wave approach proposed is verified by the fact that both curves show not only (i) the same sequence of main extremes (maxima, minima), but also (ii) at very close frequency values, even identical for certain ones. As far as time efficiency of the specific implementation is concerned, computation of the simulated curve in Figure 4 took on a PC with a Dual Core 1.66 GHz processor and 1 GB of RAM no longer than 2 min, comprising selection and complete determination (amplitude, phase, real part and imaginary part) of some hundreds paths for each of 235 frequency values uniformly allocated from 1.6 MHz to 25 MHz at steps of 100 kHz.

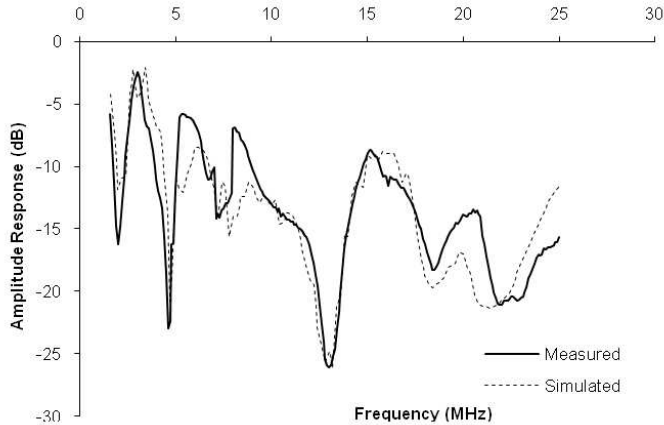


**Figure 4.** Results of experimental evaluation.

### 3. APPLICABILITY

#### 3.1. Bandwidth — Variation with Frequency

The analysis elaborated in this work applies directly to narrowband signalling in terms of the actual spectral configuration of the transmitted signal(s). A multicarrier wideband transmission technique like the highly promising Orthogonal Frequency Division Multiplexing (OFDM) should therefore be treated on narrowband signalling basis, since it would normally involve no transmission of wideband signals, but consist in dividing the data stream into several sub-streams transmitted over equally numbered narrowband sub-channels configured that narrow to ensure distortionless transmission [5]. As long as the delay spread, usually represented by the root mean square (RMS) delay spread parameter ( $\tau_{rms}$ ) defined as the second central moment of channel's power delay profile [6], keeps sufficiently short compared with the symbol duration, each one of the actual sub-signals transmitted within a multicarrier scheme may in fact be treated as narrowband signalling directly suitable for the present travelling-wave approach.

Although either inherently wideband transmission is performed — e.g., Direct Sequence Spread Spectrum (DSSS) — or simply the bandwidth of the transmitted continuous-wave modulated signal is broader than what would justify a narrowband approach, the path amplitude and arrival-time quantities can be extrapolated via proper

weighted averaging or vectorial summation of the several narrowband homologous components [6, 7], and then RMS delay spread may be calculated. As though the latter is a central moment of the power delay profile, a simple direct recipe, though further approximative, would extract the wideband  $\tau_{rms}$  as a weighted average of the narrowband  $\tau_{rms}$  values utilising as weighting function the energy spectral density of the signal transmitted, whereupon the derived frequency variation of  $\tau_{rms}$  would as well be of direct applicability.

From a purely computational point of view, if either wideband or multi-carrier transmission is applied, travelling-wave simulation must be repeated for every carrier frequency under investigation substituting for each one the corresponding MTL parameters' values. If however modal decomposition of the line is not frequency-independent, the eigenvector-eigenvalue routine for complex matrices that provides the transformation matrices  $\hat{\mathbf{T}}_V$  and  $\hat{\mathbf{T}}_I$  must be repeatedly called at every carrier frequency, causing therefore unavoidably some additional time consumption. Nevertheless, such efficient routines for several more or less common MTL structures are already available [3].

### 3.2. Comparative Evaluation — Exploitation Prospects

In relation to the existing TL and/or Power-Line Communication (PLC) channel modelling methods in the Time Domain (TD), the comparative assets of the travelling-wave approach, prioritised on the basis of novelty at first and secondly computational facilitation, are estimated as follows:

- 1) The narrowband TD response and all crucial channel performance parameters ( $\tau_{rms}$ , power delay profile, path amplitudes, arrival times etc.) are calculated not by use of any numerical transformation from the FD solution or numerical approximation of the TL network, but through analytical elaboration of the multipath propagation process that forms the actual (physical) response mechanism, so that:
  - a. Estimation of the power delay profile is exact and accurate, allowing for no erroneous results or deductions that could occur due to application of quantitative criteria or thresholds within a process involving numerical transformation or/and approximation. This was particularly demonstrated for the simplified (reduced) case of a two-conductor TL network configuration in [2], where the dominant path groups were identified and the power delay profile in terms of the path-amplitude and path-arrival-time distributions was separately examined within each dominant group of paths.

- b. It allows tracing back along the route of every single path, making it thus possible to identify the impact of any vicinal or short-range in general network configuration upon the channel response, as it was elaborated in [1] for the simplified (reduced) case of a two-conductor TL network configuration, where dependence of the power delay profile in terms of the path-amplitude and path-arrival-time distributions on the vicinal network's complexity and extent was examined.

This is considered to be the main novel contribution, which *differentiates from a telecommunications point of view the specific travelling-wave analysis from all existing TD response analysis and simulation approaches, enhancing considerably channel estimating and optimising capabilities.*

- 2) Given the network topology, the cable/TL parameters and the termination loads, it allows for completely computational simulation that requires no experimental feedback, in contrast with other similar approaches that pre-assume the response pattern and use experimental results to calibrate the pattern parameters.
- 3) Depending on the transmission and modulation schemes utilised (narrowband, wideband, multicarrier etc.), the path incorporation criterion can be properly set to select only the paths actually required, preserving thus computation time and achieving optimal efficiency.

The ideally exploitable final product of this work would be an efficient and accurate computational algorithm that would cover wholly the general MTL case and all the reduced sub-cases, allowing channel analysis both with modulation/transmission performance estimation and optimisation over any PLC network, and with applicability to other MTL channel structures as well, as generalised as possible. Such an algorithm is anticipated to be the output of ongoing research, and will in addition offer a pure, intact field for the study of related complexity and error-analysis issues.

#### 4. CONCLUSION

In Part II of this work, a validating example has in principle been presented for the travelling-wave analysis of uniform multi-conductor transmission line networks that was theoretically established in Part I, involving comparative evaluation between the measured and simulated amplitude responses of an actual branched-bus arrangement of multi-conductor power cables.

Given that the travelling-wave approach introduced in this work is directly applicable to narrowband transmission and only if diagonal modal decomposition of the involved transmission lines is indeed feasible, further related research is in particular suggested on (i) efficient algorithms implementing computationally the travelling-wave analysis to simulate network response in the time domain and extract the desired performance parameters, (ii) proper combination of spectral segmentation with integration and/or other appropriate numerical/statistical techniques in order to approach treatment of wideband signalling, and (iii) possible expansion of the travelling-wave analysis to include the general non-diagonalisable MTL case via the quasi-diagonal block Jordan transformation.

## REFERENCES

1. Papaleonidopoulos, I. C., C. G. Karagiannopoulos, I. E. Anagnostopoulos, and N. J. Theodorou, "An HF multipath-propagation analysing method for power delay profile estimations of indoor single — phase low voltage PLC channels," *Proc. 7th Int. Symp. Power-Line Communications and Its Applications (ISPLC2003)*, 154–159, Kyoto, Japan, 2003.
2. Papaleonidopoulos, I. C., C. G. Karagiannopoulos, and N. J. Theodorou, "Travelling-wave multipath simulation of two-conductor HF signalling over indoor power-line networks and RMS-delay-spread dependence," *Europ. Trans. Telecommunications*, Vol. 18, 275–285, 2007.
3. Paul, C. R., *Analysis of Multiconductor Transmission Lines*, 46–76, 92–93, 164–168, 157–180, 186–230, John Wiley & Sons, Inc., New York, 1994.
4. Papaleonidopoulos, I. C., C. G. Karagiannopoulos, and N. J. Theodorou, "Evaluation of the two-conductor HF transmission-line model for symmetrical indoor triple-pole cables," *Measurement*, Vol. 39, 719–728, 2006.
5. Haykin, S., *Communication Systems*, 4th Edition, 431–448, 535–542, John Wiley & Sons, Inc., New York, 2000.
6. Pahlavan, K. K. and A. H. Levesque, *Wireless Information Networks*, 42–60, 73–74, John Wiley & Sons, Inc., New York, 1995.
7. Hashemi, H., "The indoor radio propagation channel," *Proceedings of the IEEE*, Vol. 81, 941–968, 1993.